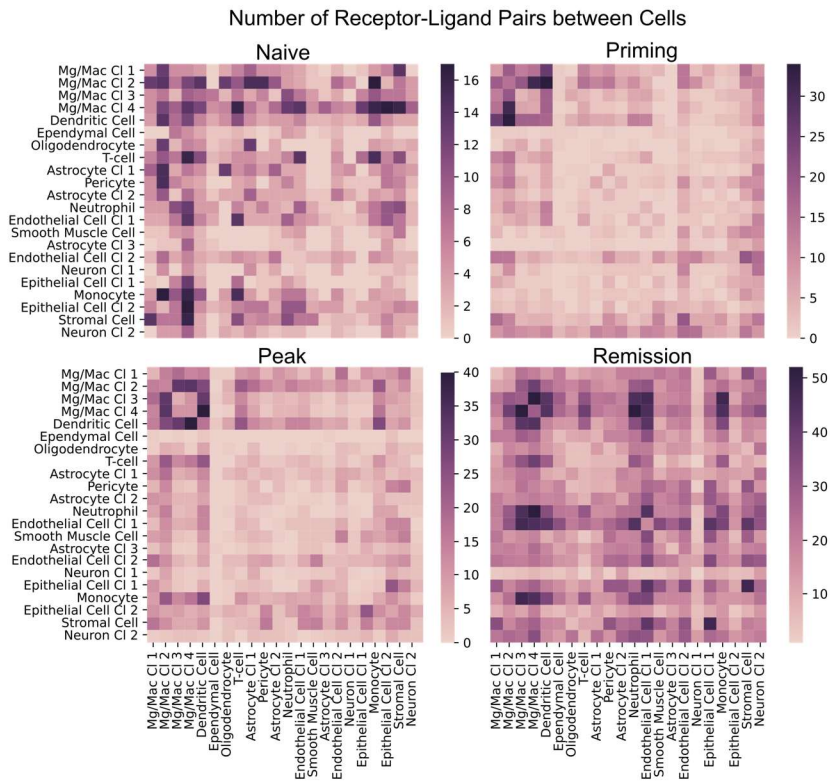
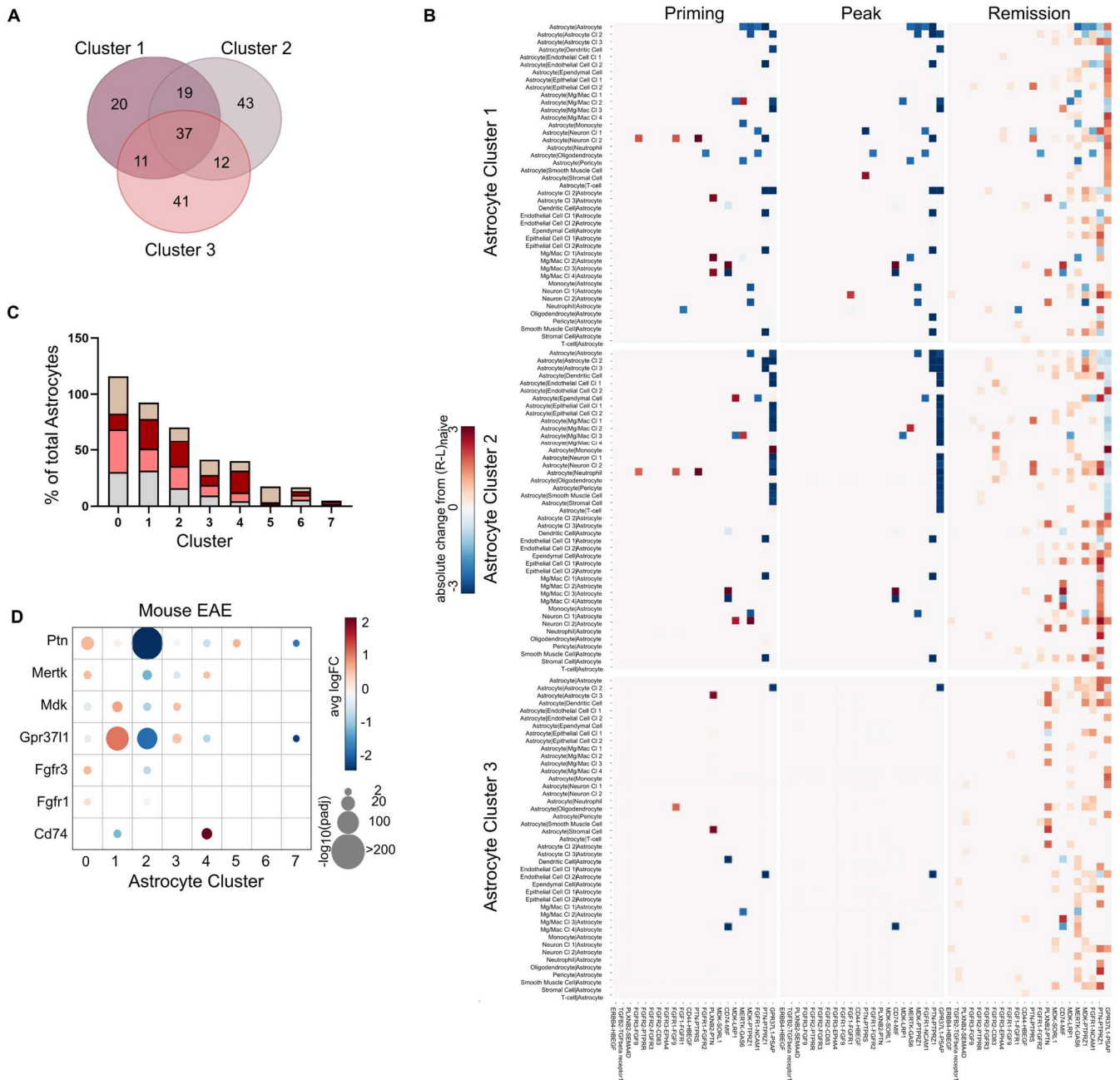


1 **Supplementary Table 1.**

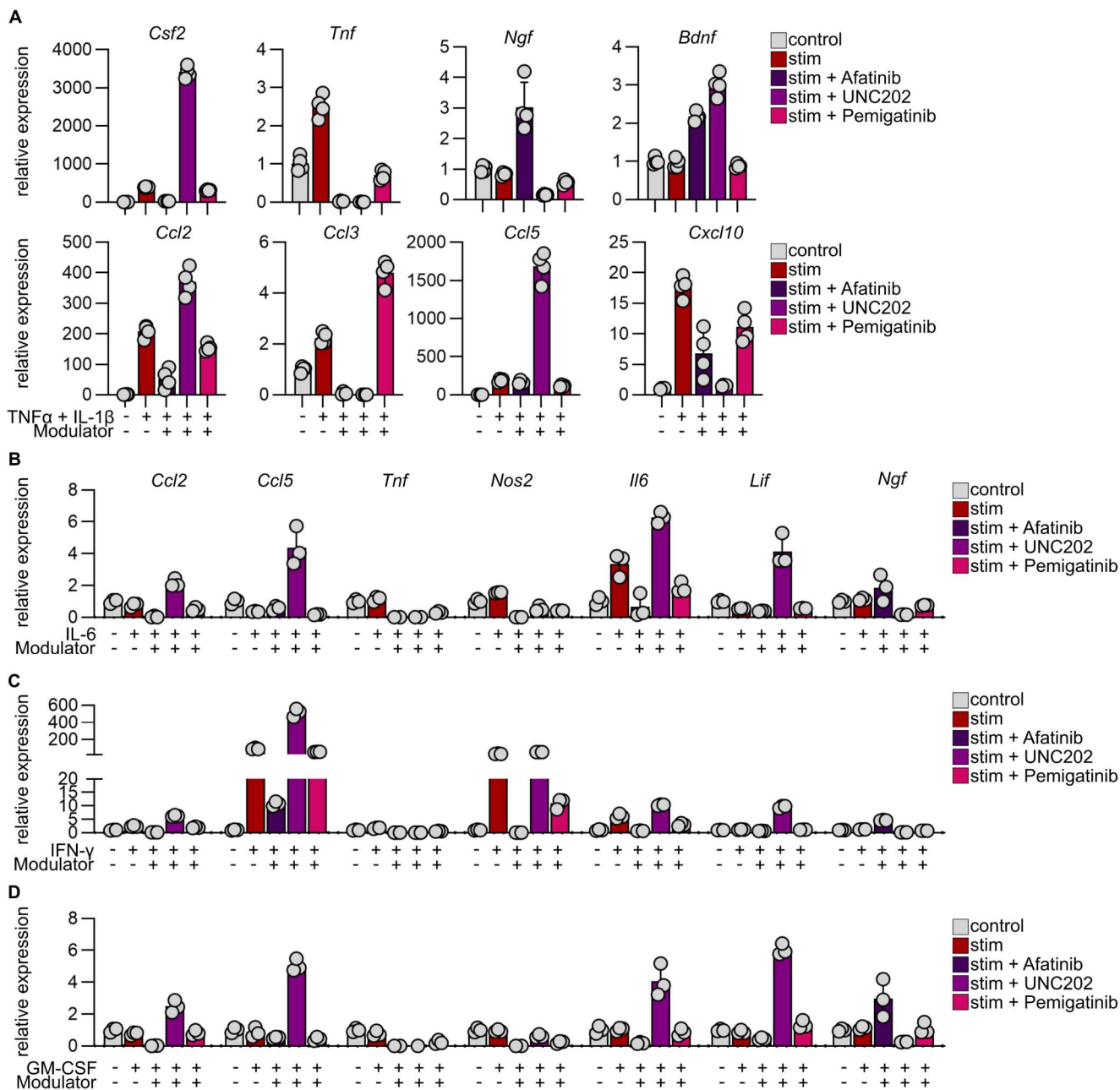
<b>Agent</b>	<b>Target</b>	<b>Indication</b>
Afatinib	ErbB1, ErbB2, ErbB4	Non-small cell lung cancer (30)
Dacomitinib	ErbB1, ErbB2, ErbB4	Non-small cell lung cancer (31)
Erdafitinib	pan-FGFR, RET (c-RET), CSF-1R, PDGFR- $\alpha$ /PDGFR- $\beta$ , FLT4, VEGFR-2	urothelial cancer, metastatic or locally advanced bladder cancer (32)
Ponatinib	FGFR1, Abl, PDGFR $\alpha$ , VEGFR2	Chronic myeloid leukemia, acute lymphoblastic leukemia (33)
Pemigatinib	FGFR1, FGFR2, FGFR3, FGFR4	Advanced cholangiocarcinoma (34)
Proglumide	CCK <sub>A</sub> , CCK <sub>B</sub>	-
Prosaptide TX14(A)	GPR37L1	-
UNC2025	MERTK, FLT3	-
MDK	ALK, LRP1, LRP2, PTPRZ1, NOTCH2	-
PTN	ALK, PTPRZ1, LRP1, Nucleolin	-
MIF	CD74, CD44, CXCR2	-



**Supplementary Figure 1. Absolute number of cell-cell receptor-ligand interactions throughout EAE progression.** Number of inferred receptor-ligand pairs between cell types in the naïve, priming, peak and remission stage of EAE identified in scRNA-Seq by (8) after using the CellPhoneDB algorithm (11).

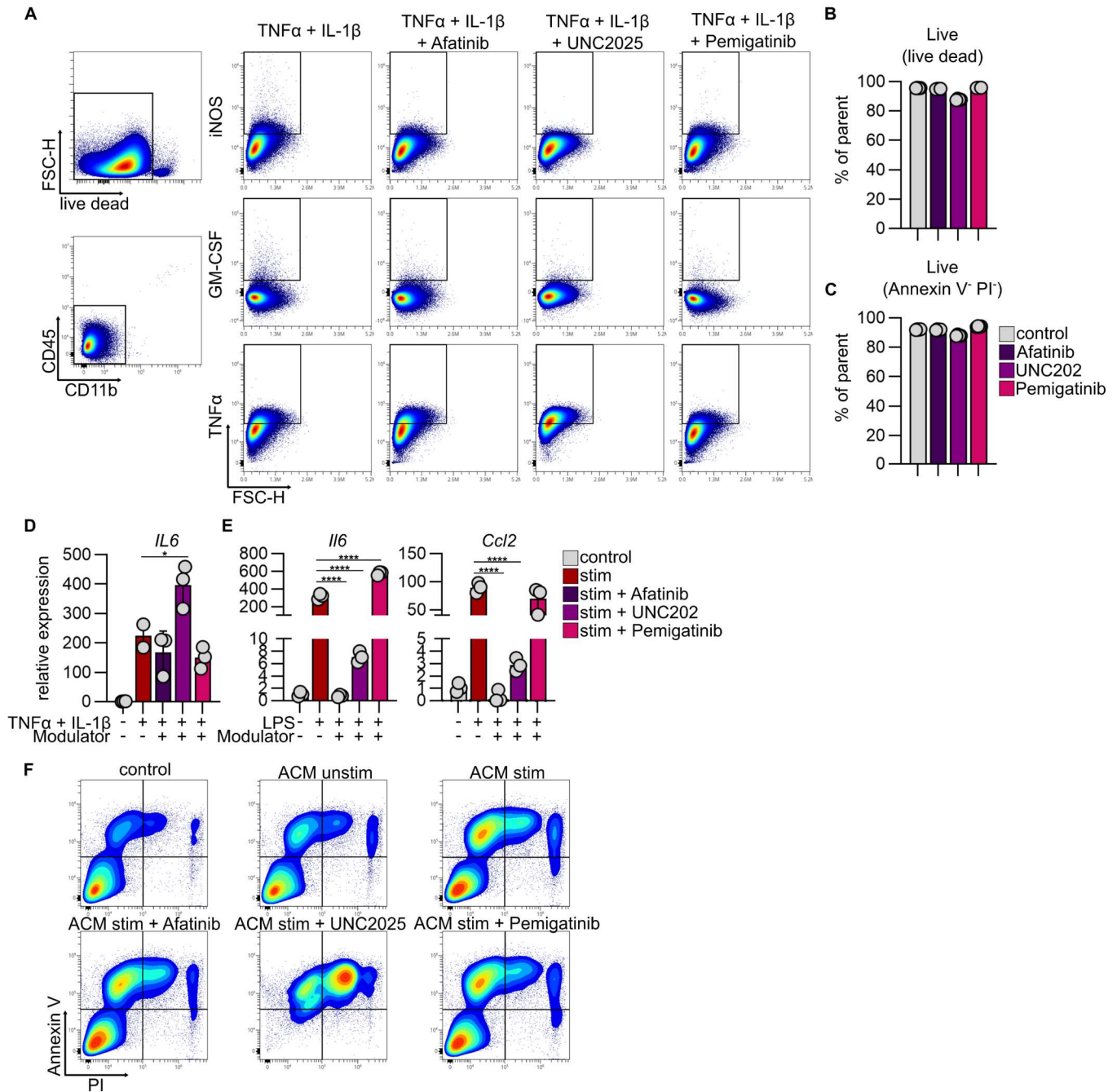


**Supplementary Figure 2. Inferred receptor-ligand interactions formed by astrocyte clusters during EAE. (A)** Venn diagram of receptor-ligand interactions formed by astrocyte clusters identified in Wheeler et al. (8). **(B)** Absolute changes  $((R-L)_{stage} - (R-L)_{naive})$  in co-expression of curated receptor-ligand pairs formed by astrocyte clusters throughout EAE. Positive changes indicate upregulation compared to naïve stage. **(C)** Abundance of astrocyte subclusters from (8) based on per cent composition in EAE and their expression of curated receptors and ligands **(D)**.



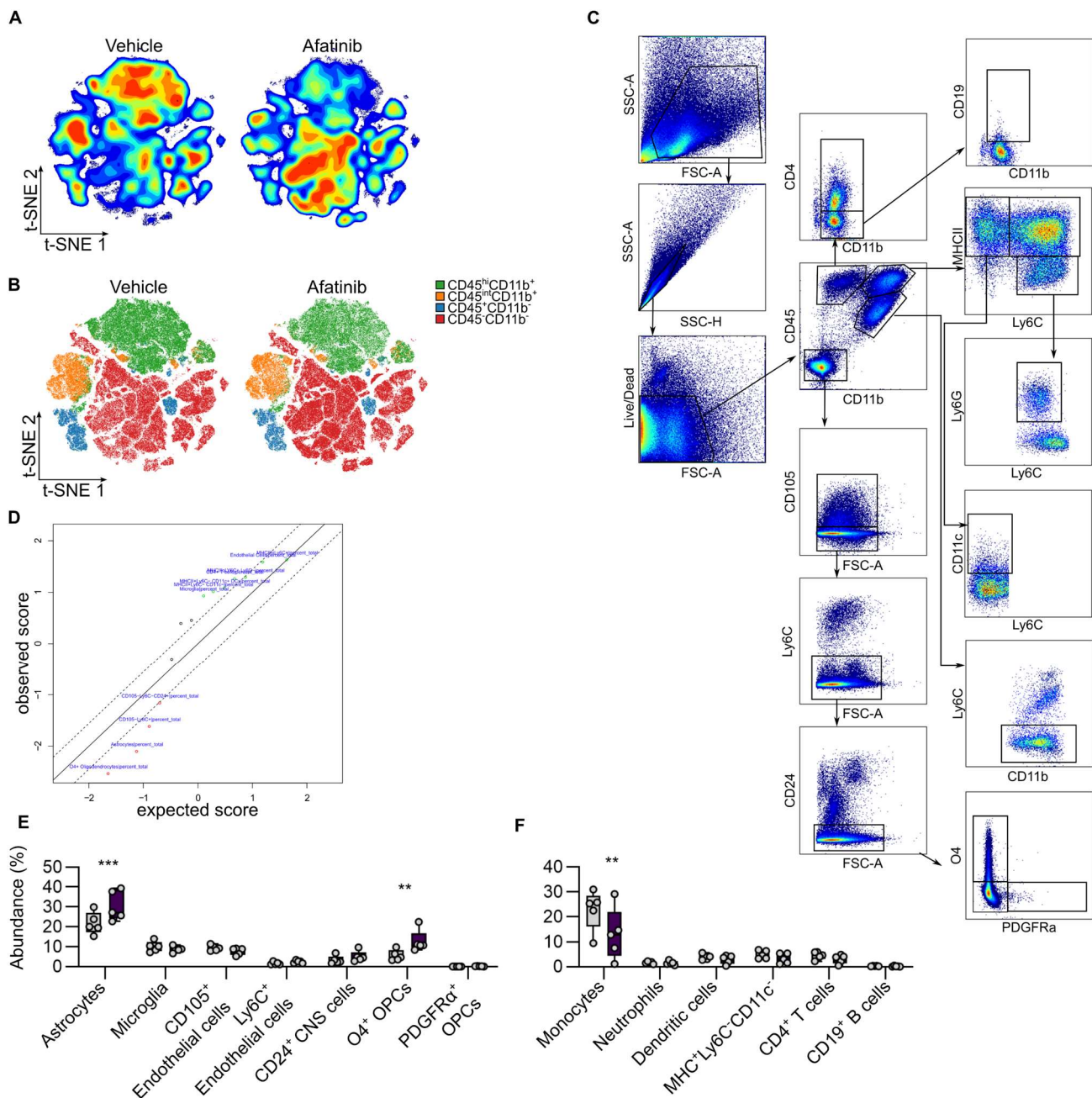
**Supplementary Figure 3. Afatinib, UNC2025, and Pemigatinib regulate inflammatory properties of astrocytes *in vitro*.** (A) Relative expression of *Csf2*, *Tnf*, *Ngf*, *Bdnf*, *Ccl2*, *Ccl3*, *Ccl5*, *Cxcl10* quantified by RT-qPCR in primary mouse astrocytes following stimulation with vehicle or TNF $\alpha$  + IL-1 $\beta$   $\pm$  Afatinib, UNC2025, Pemigatinib; n = 4 per group; Two-way ANOVA with Dunnett's multiple comparisons test. Data representative for n = 3 independent experiments. (B) Relative expression of *Ccl2*, *Ccl5*, *Tnf*, *Nos2*, *Il6*, *Lif*, and *Ngf* quantified by RT-qPCR in primary mouse astrocytes following stimulation with vehicle or IL-6, IFN- $\gamma$  (C), or GM-CSF (D)  $\pm$  Afatinib, UNC2025, Pemigatinib; n = 3 per group; Two-way ANOVA with Dunnett's multiple comparisons test.

## Supplementary Figure 3

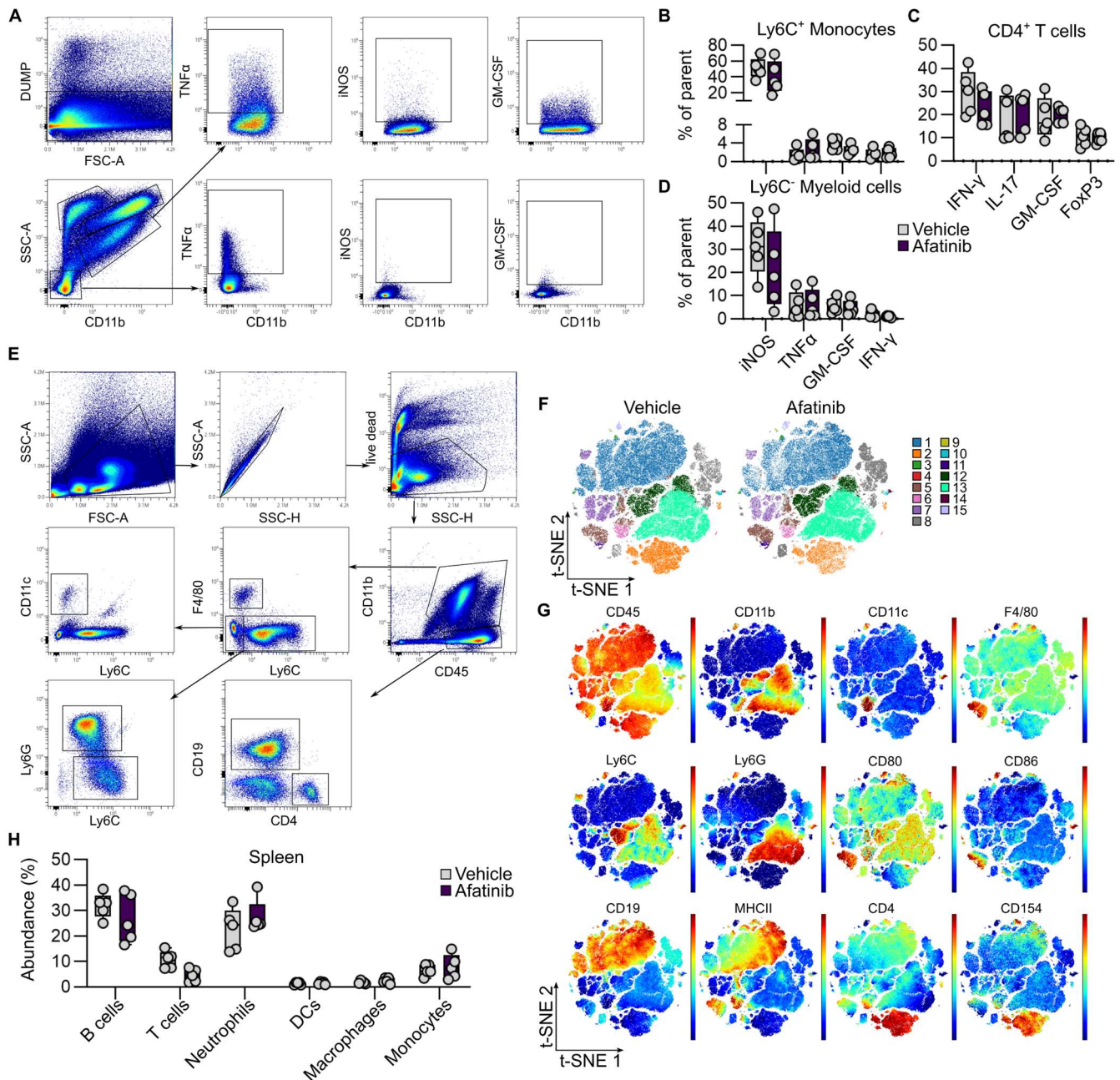


**Supplementary Figure 4. Functional assessment of Afatinib, UNC2025, and Pemigatinib on glial and neuronal cells *in vitro*.** (A) Representative scatter plots for intracellular flow cytometry measurements of TNF $\alpha$ , IL-1 $\beta$ , and GM-CSF in primary mouse astrocytes following stimulation with TNF $\alpha$  + IL-1 $\beta$   $\pm$  Afatinib, UNC2025 and Pemigatinib. (B) Quantification of amine-dependent and Annexin V (AV) / Propidium Iodid (PI) (C) live dead staining of primary mouse astrocytes following stimulation with vehicle, Afatinib, UNC2025 and Pemigatinib;  $n = 4$  per group. (D) *IL6* expression quantified by RT-qPCR in human astrocytes  $\pm$  stimulation with TNF $\alpha$  + IL-1 $\beta$   $\pm$  Afatinib, UNC2025 and Pemigatinib;  $n = 3$  per group; One-way ANOVA with Dunnett's multiple comparisons test. (E) *IL6*, and *Ccl2* expression quantified by RT-qPCR in primary mouse microglia  $\pm$  stimulation with LPS  $\pm$  Afatinib, UNC2025 and Pemigatinib;  $n = 3$  per group; One-way ANOVA with Dunnett's multiple comparisons test. (F) Representative scatter plots for Annexin V (AV) Propidium Iodid (PI) apoptosis assay of N2A neuronal cells following stimulation with astrocyte-conditioned medium (ACM). \*  $P < 0.05$ ; \*\*\*\*  $P < 0.0001$ .

## Supplementary Figure 4

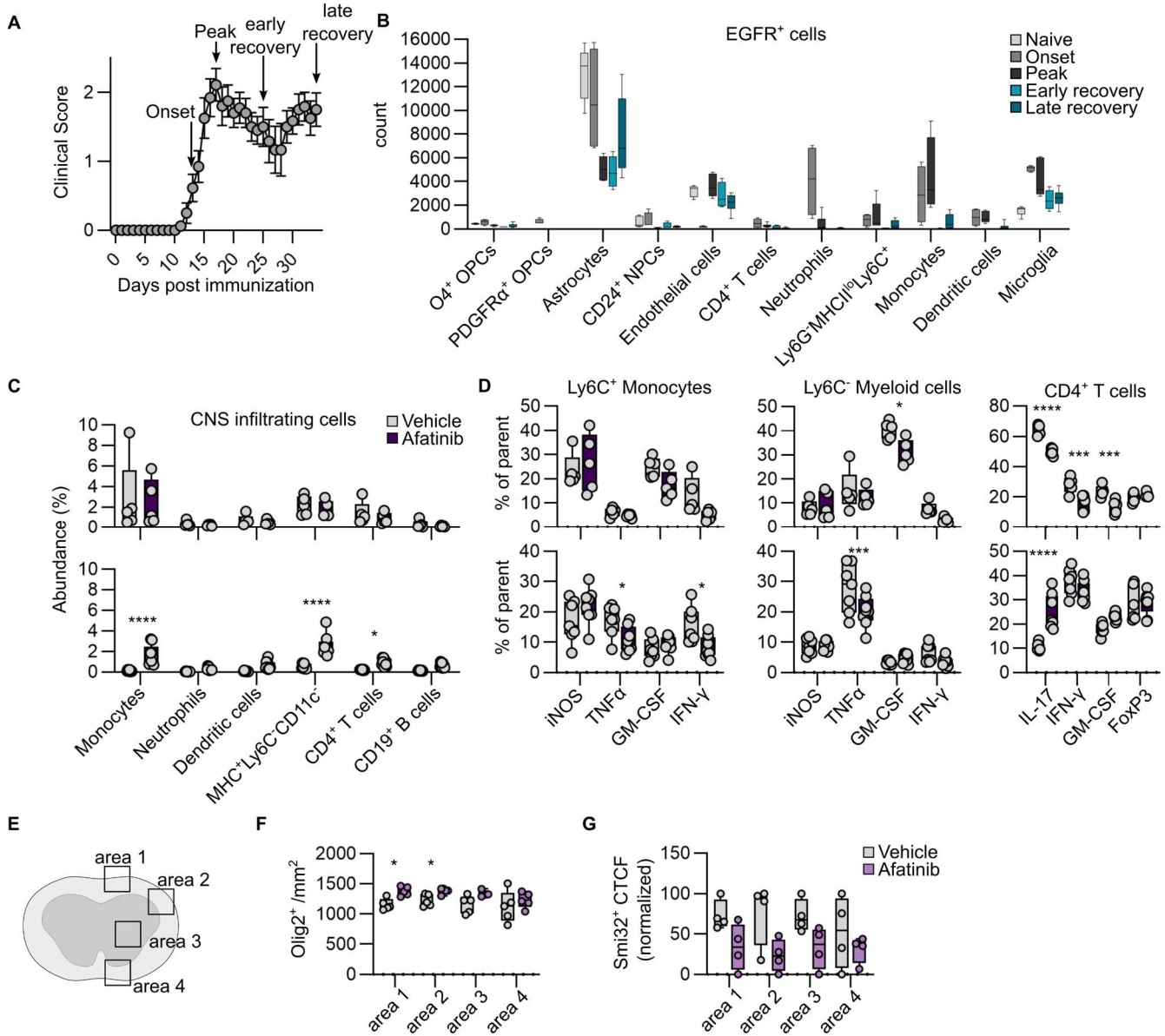


**Supplementary Figure 5. Intranasal delivery of Afatinib modulates cellular composition in the CNS during acute stages of EAE.** (A) Unsupervised clustering t-distributed stochastic neighbour embedding (t-SNE) plot of CNS cells during acute neuroinflammation obtained from mice treated intranasally with vehicle ( $n = 5$ ) or Afatinib ( $n = 5$ ) from symptom onset. (B) t-SNE plot with cellular clusters based on CD45 and CD11b expression of CNS cells obtained from mice treated with Afatinib ( $n = 5$ ) or vehicle ( $n = 5$ ) at peak of disease. (C) Gating strategy used to identify cell populations in the CNS based on their surface expression of cellular markers. (D) SAM plot of significantly differing cell populations in the CNS of mice treated with Afatinib ( $n = 5$ ) or vehicle ( $n = 5$ ) at peak of EAE. (E) CNS-intrinsic and -infiltrating (F) cell populations in the CNS of mice treated with Afatinib ( $n = 5$ ) or vehicle ( $n = 5$ ) at peak of EAE. Two-way ANOVA with Sidak's multiple comparisons test. \*\*  $P < 0.01$ ; \*\*\*  $P < 0.001$ .

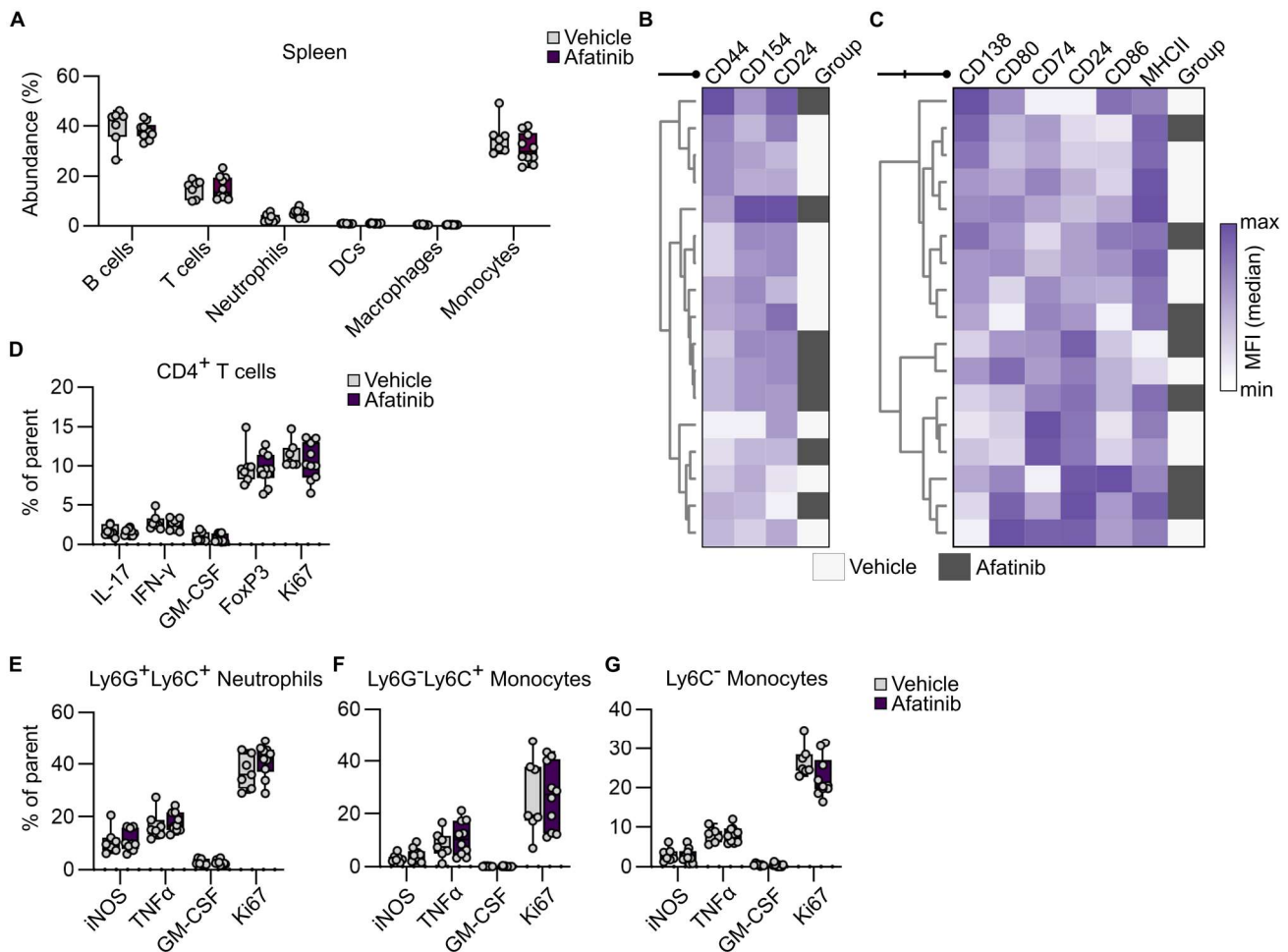


**Supplementary Figure 6. Intranasal delivery of Afatinib alters the inflammatory phenotype of cells in the CNS but not the periphery . (A)** Gating strategy used for the quantification of cytokines produced by microglia (top) and astrocytes (bottom) by intracellular flow cytometry. DUMP<sup>-</sup> cells (Ter-119<sup>-</sup>, B220<sup>-</sup>, CD140a<sup>-</sup>, O4<sup>-</sup>, Ly6G<sup>-</sup>, Ly6C<sup>-</sup>) cells were gated after exclusion of dead cells by amine-dependent live dead staining. **(B)** Relative expression of intracellular cytokines and intranuclear markers in CD45<sup>hi</sup>CD11b<sup>+</sup>Ly6C<sup>+</sup> monocytes, CD45<sup>+</sup>CD11b<sup>-</sup>CD4<sup>+</sup> T cells **(C)**, and CD45<sup>hi</sup>CD11b<sup>+</sup>Ly6C<sup>-</sup> myeloid cells **(D)** in the CNS of mice treated with Afatinib (n = 5) or vehicle (n = 5) at peak of EAE measured by intracellular flow cytometry. **(E)** Gating strategy used to identify splenic cell populations based on their surface expression of cellular markers. **(F)** Unsupervised clustering t-distributed stochastic neighbour embedding (t-SNE) plot overlaid with clusters identified by FlowSOM-clustering of splenic cells measured by high-dimensional flow cytometry in mice treated intranasally with vehicle (n = 5) or Afatinib (n = 5) from symptom onset. **(G)** Median fluorescence intensity (MFI) of surface markers expressed by splenic cell clusters at peak of EAE. **(H)** Abundance of splenic cell populations in mice treated intranasally with vehicle (n = 5) or Afatinib (n = 5) from symptom onset following manual gating.

## Supplementary Figure 6



**Supplementary Figure 7. Intranasal delivery of Afatinib ameliorates late stage CNS inflammation .** (A) EAE development and clinical course in WT B6 mice; arrows indicate sampled timepoints. Data are shown as mean  $\pm$  SEM. (B) Epidermal growth factor receptor (EGFR) expression on cell populations in the CNS of naïve mice (n = 5), during onset (n = 4), peak (n = 6), early- (n = 4) or late recovery (n = 8) stages of EAE, measured by high-dimensional flow cytometry. (C) Abundance of CNS infiltrating cells during late stage CNS inflammation in mice treated with vehicle or Afatinib from symptom onset (vehicle n = 5, Afatinib n = 5) (top) or peak of disease (vehicle n = 7, Afatinib n = 8) (bottom); Two-way ANOVA with Sidak's multiple comparisons test. (D) Relative expression of cytokines and intranuclear markers in CD45<sup>hi</sup>CD11b<sup>+</sup>Ly6C<sup>+</sup> monocytes, CD45<sup>hi</sup>CD11b<sup>+</sup>Ly6C<sup>-</sup> myeloid cells, and CD45<sup>hi</sup>CD11b<sup>+</sup>CD4<sup>+</sup> T cells measured by intracellular flow cytometry in the CNS of mice treated with vehicle or Afatinib from symptom onset (vehicle n = 5, Afatinib n = 5) (top) or peak of disease (vehicle n = 7, Afatinib n = 8) (bottom) during late stage CNS inflammation. Two-way ANOVA with Sidak's multiple comparisons test. (E) Schematic of the areas samples for IHC quantification in lumbar spinal cord sections. (F) Quantification of immunohistochemically labelled Olig2<sup>+</sup> oligodendrocytes and axonal damage (SMI32<sup>+</sup>) in lumbar spinal cord of mice treated with vehicle (n = 5) or Afatinib (n = 5) during late stage CNS inflammation. Two-way ANOVA with Sidak's multiple comparisons test. \*  $P < 0.05$ ; \*\*\*  $P < 0.001$ ; \*\*\*\*  $P < 0.0001$ .



**Supplementary Figure 8. Effect of Afatinib on splenic cells during late stage CNS inflammation.** (A) Abundance of major immune cell populations in the spleen of mice treated with vehicle ( $n = 7$ ) or Afatinib ( $n = 9$ ) from peak of disease, measured by high-dimensional flow cytometry. (B) Euclidian clusterin based on normalized median fluorescence intensity (MFI) of activation markers expressed on T cells and myeloid cells (C) during late stage CNS inflammation in mice treated with vehicle ( $n = 7$ ) or Afatinib ( $n = 9$ ) from peak of disease, measured by high-dimensional flow cytometry. (D) Relative expression of cytokines and intranuclear markers during late stage CNS inflammation in CD45<sup>+</sup>CD11b<sup>-</sup>CD4<sup>+</sup> T cells, CD45<sup>hi</sup>CD11b<sup>+</sup>Ly6C<sup>+</sup>Ly6G<sup>+</sup> neutrophils (E), CD45<sup>hi</sup>CD11b<sup>+</sup>Ly6C<sup>+</sup>Ly6G<sup>-</sup> monocytes (F), and CD45<sup>hi</sup>CD11b<sup>+</sup>Ly6C<sup>-</sup> myeloid cells (G) in spleens of mice treated with vehicle ( $n = 7$ ) or Afatinib ( $n = 9$ ) from peak of disease.